Journal of Biomedical Optics

BiomedicalOptics.SPIEDigitalLibrary.org

Micron resolution, high-fidelity three-dimensional vascular optical imaging phantoms

Callum D. Little
Radhika K. Poduval
Richard Caulfield
Sacha Noimark
Richard J. Colchester
Chris D. Loder
Manish K. Tiwari
Roby D. Rakhit
Ioannis Papakonstantinou
Adrien E. Desjardins

SPIE.

Callum D. Little, Radhika K. Poduval, Richard Caulfield, Sacha Noimark, Richard J. Colchester, Chris D. Loder, Manish K. Tiwari, Roby D. Rakhit, Ioannis Papakonstantinou, Adrien E. Desjardins, "Micron resolution, high-fidelity three-dimensional vascular optical imaging phantoms," *J. Biomed. Opt.* **24**(2), 020502 (2019), doi: 10.1117/1.JBO.24.2.020502.

Micron resolution, high-fidelity three-dimensional vascular optical imaging phantoms

Callum D. Little,[a,b,†] Radhika K. Poduval,[c,d,†] Richard Caulfield,[a,d,e] Sacha Noimark,[a,d] Richard J. Colchester,[a,c] Chris D. Loder,[b] Manish K. Tiwari,[a,e] Roby D. Rakhit,[b] Ioannis Papakonstantinou,[c,*] and Adrien E. Desjardins[a,d,*]

[a]Wellcome Trust–EPSRC Centre for Interventional and Surgical Sciences, London, United Kingdom
[b]Royal Free Hospital, Department of Cardiology, London, United Kingdom
[c]University College London, Department of Electronic and Electrical Engineering, Photonic Innovations Lab, London, United Kingdom
[d]University College London, Department of Medical Physics and Bioengineering, London, United Kingdom
[e]University College London, Nanoengineered Systems Laboratory, UCL Mechanical Engineering, London, United Kingdom

Abstract. Microscopic and mesoscale optical imaging techniques allow for three-dimensional (3-D) imaging of biological tissue across millimeter-scale regions, and imaging phantom models are invaluable for system characterization and clinical training. Phantom models that replicate complex 3-D geometries with both structural and molecular contrast, with resolution and lateral dimensions equivalent to those of imaging techniques (<20 μm), have proven elusive. We present a method for fabricating phantom models using a combination of two-photon polymerization (2PP) to print scaffolds, and microinjection of tailored tissue-mimicking materials to simulate healthy and diseased tissue. We provide a first demonstration of the capabilities of this method with intravascular optical coherence tomography, an imaging technique widely used in clinical practice. We describe the design, fabrication, and validation of three types of phantom models: a first with subresolution wires (5- to 34-μm diameter) arranged circumferentially, a second with a vessel side-branch, and a third containing a lipid inclusion within a vessel. Silicone hybrid materials and lipids, microinjected within a resin framework created with 2PP, served as tissue-mimicking materials that provided realistic optical scattering and absorption. We demonstrate that optical phantom models made with 2PP and microinjected tissue-mimicking materials can simulate complex anatomy and pathology with exquisite detail. [DOI: 10.1117/1.JBO.24.2.020502]

Keywords: optics; two-photon polymerization; imaging phantoms; optical coherence tomography; tissue-mimicking materials; vascular.

Paper 180574LR received Oct. 5, 2018; accepted for publication Jan. 8, 2019; published online Feb. 15, 2019.

*Address all correspondence to Ioannis Papakonstantinou, E-mail: i.papakonstantinou@ucl.ac.uk; Adrien E. Desjardins, E-mail: a.desjardins@ucl.ac.uk

†Callum D. Little and Radhika K. Poduval contributed equally to this work.

With the proliferation of new microscopic and mesoscopic imaging techniques, there is a crucial need for new fabrication methods to create suitably sized phantom models with three-dimensional (3-D) tissue architectures and variations in molecular composition. Phantom models with simple geometries enable system characterization and clinical training, ensuring both the reliability and reproducibility of data collected, and reducing inconsistency and systematic errors.[1] High-fidelity, complex, and miniature phantom models are required to guide image interpretation and appreciation of how different anatomical structures can present with a given imaging technique. To simulate anatomical structures, inclusion of both structural and molecular sources of contrast into predefined geometrical locations within the phantom model is of particular importance. Manufacturing microscale-resolution phantoms would require a combination of high-resolution manufacturing techniques to fabricate a scaffold model and include appropriate contrast. Optical coherence tomography is an example of a mesoscale imaging technique with multiple clinical applications for which phantom model development has been particularly challenging. Within the field of interventional cardiology, intravascular optical coherence tomography (IVOCT) is performed with a miniature probe [outer diameter (OD): 0.9 mm] that is inserted into the vasculature. Imaging is performed by rapidly rotating and translating a focused beam that typically penetrates tissue at depths of 1 to 2 mm. It is of importance to understand how the visibility of a small structure may vary across the image. Ideally, an imaging phantom for IVOCT would provide multiple elements of varying sizes, including subresolution targets at multiple distinct spatial locations. This could allow for quantifying image distortions due to nonuniform rotation and subsampling in the angular domain. Interpretation of IVOCT images is often difficult,[2] given that its spatial resolution (axial/lateral: typically 10/20 μm) is close to that of cell diameters, and images are confounded by speckle noise. Two examples of vascular tissue structures of particular interest to simulate in phantom models are vessel side-branches and lipid-rich plaques that can rupture and cause myocardial infarctions (referred to commonly as a "heart attack").

With current methods used to fabricate phantom models for IVOCT system performance characterization, it remains challenging to precisely position subresolution sized scattering structures at a range of different depths and orientations. The most commonly described method involves imaging of subresolution sized particles, such as silica microspheres, iron oxide, and gold-silica nanoshells.[3,4] This technique relies on integration of particles within a polymer mixture and they therefore have a random spatial distribution; moreover, aggregation of these particles and imperfections within the polymer may also lead to measurement variability. Vascular structures can be complex, with multiple structural components at different orientations, and it is of great interest to replicate these heterogeneities in imaging phantoms. Significant progress has been made to create materials with optical scattering and absorption properties similar to vascular tissue[5–13]; however, shaping these materials with heterogeneity in all dimensions and at the micron-to-millimeter size scales relevant to small arteries has been very challenging. Three-dimensional additive printing offers an alternative method for the creation of scaffolds that resemble biological structures, but not at the microscopic scale relevant to a number of anatomical structures.[14,15]

Recently, there have been significant advances in the fabrication of microscale polymeric structures through nanoscopic

additive manufacturing methods with photoresists[16–18] that have printing resolutions equivalent or superior to those of microscopic and mesoscopic imaging systems. Two photon polymerization (2PP) printing is one the most prominent of these techniques; it enables submicron scale 3-D printing to a resolution below 200 nm,[19] depending on the photoresist used. 2PP printing is realized using a tightly focused femtosecond laser beam to induce cross linking of 3-D nanostructures inside a photocurable polymer[20] through two-photon absorption[21] in a localized focal volume, which is followed by a washout of the noncrosslinked material. In this study, we aimed to investigate how 2PP printing can be used on its own and in combination with microinjection to fabricate optically heterogeneous 3-D imaging phantoms. In this hybrid method, 2PP printing is used to create mesoscale free-standing wires with subresolution lateral dimensions for circumferential resolution testing, and scaffolds into which optically scattering silicones and lipids are injected to mimic different healthy and pathological tissues.

A mesoscale wire phantom model was designed with computer-aided design (CAD) software (Fusion 360, Autodesk Inc, San Rafael, California). This comprised a central cylindrical channel with a diameter of 1 mm, through which an IVOCT imaging probe (OD: 0.9 mm) could be inserted. The wires were arranged in a circular pattern, with each wire center at a distance of 0.7 mm from the imaging channel center. Starting with the smallest wire (OD: 5 μm), the wire OD was augmented by 1-μm increments in a clockwise fashion at an angular interval of 12 deg to reach a maximum OD of 34 μm [Fig 1(a)]. The diameter of 5 μm was chosen as the starting point as this is a factor of 2 lower than the resolution limit of our IVOCT system. Base and side plates provided structural stability. Printing with 2PP was performed with a commercial system (Photonic Professional-GT; Nanoscribe GmbH, Eggenstein-Leopoldshafen, Germany),[22] using IP-S photoresist optimized for mesoscale fabrication.[23] All 2PP fabrication was performed on indium tin oxide (ITO)-coated glass slides. After the 2PP process, the structures were developed for 90 min in propylene-glycol monomethyl-ether-acetate (PGMEA) solvent, followed by 5 min in isopropyl alcohol (IPA). After the washing off of the uncured photoresist with PGMEA, the 3-D printed structures were lifted off the ITO-glass substrate by immersing it in concentrated HCl for 5 min, followed by DI water, and then IPA for 2 min each.

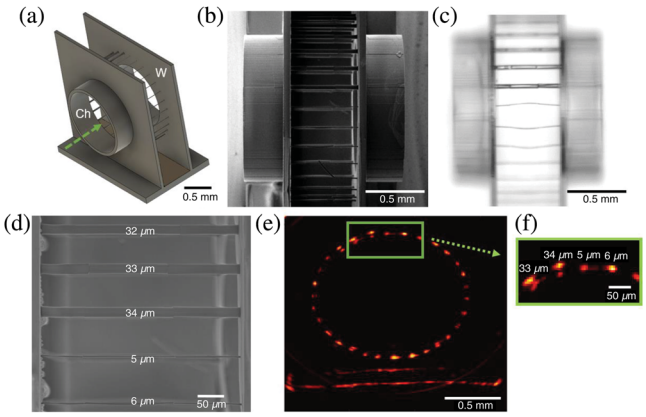

Fig. 1 (a) CAD model of the mesoscale wire phantom model. The central cylindrical channel (Ch) is circumferentially surrounded by wires (W). The dashed green arrow shows the direction of travel of the IVOCT imaging catheter. (b) SEM image of the mesoscale wire phantom model and (c) corresponding optical microscopy. (d) SEM image of the transition region that spans the thickest (34 μm) and thinnest (5 μm) wires. (e) Two-dimensional (2-D) IVOCT image with the smallest wire in the center-top position and magnified in (f).

Following 2PP printing, the mesoscale wire phantom model was secured to a glass slide using a UV-curing epoxy, which was painted onto the sides of the model with a cleaved optical fiber. The completed model was imaged under both a scanning electron microscope (SEM) [Fig. 1(b)] and an optical microscope [Fig. 1(c)] to determine the fidelity of the print and the appearance of the small wires. The transition point between the thickest (34 μm) and thinnest (5 μm) wires was well visualized on the magnified SEM image [Fig. 1(d)]. The phantom was imaged with a commercial IVOCT probe (ILLUMIEN OPTIS IVOCT imaging system and Dragonfly Duo imaging catheter; St Jude Medical, St Paul, Minnesota). This system operates in the spectral range of 1250 to 1350 nm. The imaging catheter was placed within the phantom and images were acquired in a stationary position with an acquisition speed of 180 frames per second. The sequential frames were processed using MATLAB (MathWorks, Natick, Massachusetts), to obtain a single averaged frame [Fig. 1(e)]

Using the combination of 2PP printing and microinjection, vessel side-branch phantom models can be created. The phantom model shown in Fig. 2 comprised a main vessel (OD: 1 mm; length: 2 mm) with a side branch (OD: 0.6 mm) that bifurcated from the main vessel at an angle of 45 deg. This geometry is consistent with that found in the distal coronary arteries. The vessel structures were confined within a 2-mm open-topped cube, to create a cavity into which tissue-mimicking material could be introduced around these vessel structures [Fig. 2(a)]. Following attachment to a glass side with UV-curing epoxy, optical microscopy confirmed the fidelity of the 2PP printing process [Fig. 2(b)]. The photoresist is largely transparent at the size scales of the printed structures in this study.[24] For the tissue-mimicking material, a mixture of commercially available poly(dimethyl siloxane) (PDMS) (Sylgard 184, Dow Corning, Midland, Michigan), TiO_2 nanoparticles, and silicone oil was used. To achieve tissue-like optical scattering, TiO_2 nanoparticles with a nominal primary particle size of 21 nm (13463-67-7, Sigma-Aldrich, Germany) were added with a concentration of 2 mg/ml.[25,26] The silicone oil (Silicone Thinner, SmoothOn, Bentley Advanced Materials, UK) decreased the viscosity of the mixture and allowed for easier integration into the phantom models. Sylgard 184 resin requires a reactive component to facilitate curing and this was added in a 10:10:1

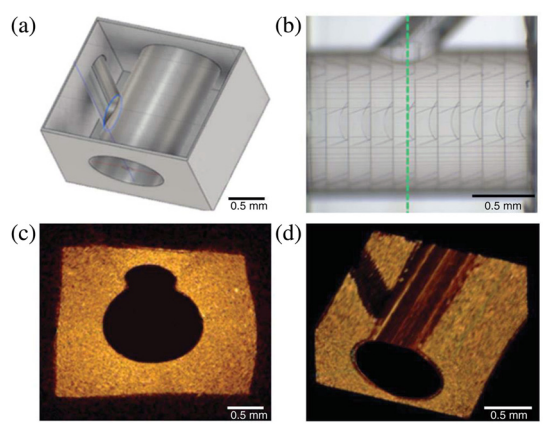

Fig. 2 (a) CAD model of the vessel side-branch phantom model and (b) corresponding optical microscopy. (c) Two-dimensional IVOCT image acquired from the side-branch region [dashed green line in (b)]. (d) 3-D IVOCT image volume.

ratio of silicone oil:PDMS resin:cross linking agent. Following mechanical mixing, the sample was sonicated for 30 min to ensure a uniform distribution of the TiO_2 nanoparticles and provide homogeneity of scattering. The mixture was then placed within a vacuum chamber for 30 min to fully allow for removal of entrapped air. Once prepared, the mixture was transferred to the scaffold using a cleaved optical fiber to deposit the material into the open-topped chamber. The integrated model was then heated to 100°C for 1 h within a convection oven, to ensure uniform curing. We imaged this completed vessel side-branch phantom model with the IVOCT system as previously described. Using an automated translation stage, an image acquisition was performed at a pullback speed of 0.89 mm/s. On the cross-sectional display, the vessel side-branch can be clearly visualized exiting the main lumen [Fig. 2(c)]. The pullback acquisition was postprocessed in a medical image viewer (Horos, Nimble Co LLC d/b/a Purview, Annapolis, Maryland) to create a 3-D reconstruction demonstrating the vessel side-branch [Fig. 2(d)].

To demonstrate how the combination of 2PP printing and microinjection can be used to simulate vascular pathology, an arterial plaque phantom model with a scaffold that replicated a lipid-rich thin capped fibroatheroma (TCFA) was fabricated. TCFAs are of major clinical interest as their presence is thought to increase the risk of developing a myocardial infarction.[27] Accurate identification of TCFAs with IVOCT is crucial, as they are not always visible with x-ray fluoroscopy. TCFAs consist of a large lipid-rich core covered by a thin fibrous cap that is <65 μm in thickness.[27] Accordingly, the CAD model for this design contained a vessel supported within a 2-mm open top cube [Fig. 3(a)]. An arc-shaped cavity close to the vessel lumen was included, thereby creating a region into which lipid could be microinjected. Outside this cavity and the vessel lumen, there was a second region in which optically scattering silicone could be introduced. This second region extended into a narrow gap between the first region and the vessel lumen; this gap represented the fibrous cap of the TCFA and was 50 μm in diameter. The silicone comprised the previously described mixture of PDMS (Sylgard 184), silicone oil, and TiO_2 was introduced into the main body of the phantom model, using a cleaved optical fiber as previously described, and then cured at 100°C for 1 h [Fig. 3(b)]. Coconut oil has a low melting point of 23°C to 27°C[28] and was, therefore, a suitable microinjectable tissue-mimicking lipid material. The aperture size of the arc-shaped cavity (<235 μm) was much smaller than that of the main compartment. In this context, micropipettes proved to be useful to precisely introduce small volumes of liquid coconut oil into the 2PP printed scaffold, under direct visualization. Glass micropipettes were manufactured using a micropipette puller (P-1000, Sutter Instrument, Novato, California). They had a tip diameter of 50 to 60 μm and a long taper of ~3 mm [Fig. 3(c)]. Luer lock adapters (EFD 15-gauge tips, Nordson, Westlake, Ohio) were fitted to the micropipettes to enable easy integration with syringes. However, in initial tests with pure glass micropipettes, injected lipids formed large droplets that built up on the outside walls of the micropipettes. This challenge was overcome by functionalizing these micropipettes using a mixture of hexane and perfluorooctyl-trichlorosilane to induce oleophobicity. The 2PP printed scaffold was mounted to an aluminum block so that the opening of the arc-shaped cavity was facing upward. A syringe containing liquid coconut oil and the attached micropipette were then positioned above the opening with a 3-axis translational stage (Thorlabs Inc, Newton, New Jersey). Using an objective lens (M Plan Apo SL 50X, Mitutoyo UK Ltd, Andover, Hampshire, UK) and a complementary metal oxide semiconductor sensor camera (DCC1545M, Thorlabs Inc, Newton, New Jersey), the position of the micropipette was monitored and adjusted [Fig. 3(d)]. The micropipette was lowered into the arc-shaped cavity and pneumatic back-pressure was applied (VPPM Proportional-pressure regulator, Festo Belgium, Brussels, Belgium) to inject liquid coconut oil from the tip [Fig. 3(e)]. The micropipette was gradually raised during filling of this region. When the coconut oil meniscus reached the top of the cavity, the pneumatic back-pressure was removed, and the micropipette was fully extracted. Once this transfer was completed, the phantom model was cooled to 4°C to allow the coconut oil to solidify before imaging. This completed lipid plaque phantom model was imaged using the same method as used for the vessel side-branch phantom model. On the cross-sectional IVOCT image, the lipid region presented as a hypoechoic area and there was slight shadowing behind this region that likely resulted from optical absorption by the lipid [Fig. 3(f)]. This appearance of microscale regions with distinct optical contrast is consistent with the molecular distribution that would be expected within a diseased vascular structure.

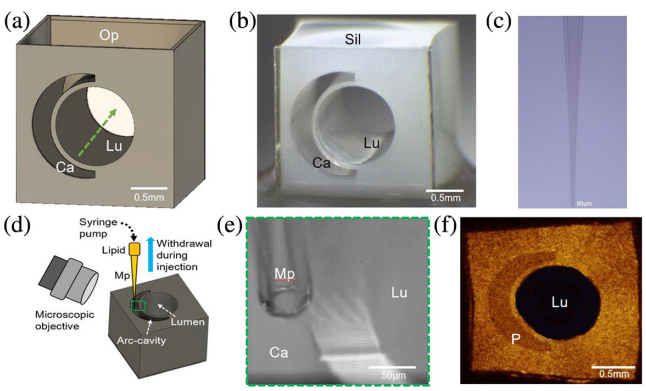

Fig. 3 (a) CAD model of the arterial plaque phantom model. The main lumen (Lu) accommodates the IVOCT catheter, with the green dashed arrow representing the direction of catheter pullback. The open-topped cavity (Op) provides an area into which an optically scattering silicone can be introduced as a tissue-simulating material. The arc-cavity (Ca) allows for introduction of lipid inclusion. (b) Optical microscopy of the model, after the main body was filled with optically scattering silicone (Sil), where the main lumen (Lu) and the arc-cavity (Ca) are unfilled. (c) Optical microscopy of the glass micropipette. Tip diameter is 50 to 60 μm with a long taper of ~3 mm. (d) Schematic showing injection of liquid coconut oil, as the arterial plaque lipid, via a functionalized micropipette (Mp) into the arc-cavity. (e) Optical microscopy of the dashed green region in (d), showing the micropipette (Mp) positioned above the arc-cavity (Ca) prior to injection. (f) Two-dimensional IVOCT image of the phantom model, in which arterial plaque (P) presents as a region with decreased scattering and with shadowing farther from the lumen center.

Manufacturing phantom models using a combination of 2PP printed scaffolds and injection of tissue-mimicking materials offers several key advantages. 2PP printing allows for highly complex vascular geometries to be simulated, and injection using the functionalized micropipettes described here allows for a high level of optical heterogeneity. Here, we have demonstrated a phantom model with a single vessel side-branch; however, multiple branches of differing sizes and orientations can be included. Patient-specific geometries can be imported from high-resolution clinical imaging modalities and used to generate freeform designs. These designs can be readily shared in digital form. Once cured, the fabricated phantom models were robust,

allowing repeated imaging with no apparent damage from the IVOCT imaging catheters after a period of 3 months, even with contact between the catheter and the wall of the central cylindrical channel. The smallest feature in the mesoscale wire phantom was 5 μm in diameter, to serve as a point target for IVOCT. However, 2PP printing has the potential to print structures as small as 200 nm or lower, which will be useful for higher resolution imaging techniques. For extended, wire-like structures, it can be useful to limit the aspect ratio to achieve structural stability. The refractive index of the printing material used here (1.49 in the NIR spectral range)[29] is higher than that of tissue (ca. 1.36 to 1.4)[30]; therefore, brighter boundaries would be expected on imaging these phantoms. This effect could be mitigated by imaging within fluids that have higher refractive indices. 2PP fabrication of mesoscale structures can be achieved for photosensitive materials with refractive index in the range of 1.3 to 1.54[31] enabling use of photoresists with specifically tailored refractive indices to match the optical characteristics of tissue. There is strong potential for directly printing heterogenous anatomical phantoms containing multiple photosensitive materials with different optical properties. Additionally, the spatial resolution of 2PP printing will enable fabrication of complex capillary networks for fluid flow phantoms, which are relevant to a wide range of imaging techniques.[32] Further, physiological phantom models suitable for florescence imaging are possible through the introduction of fluorophores or fluorescence-labeled cells into precision fabricated mesoscale structures.[33] The combination of optically generated 3-D scaffolds and microinjection of tissue-mimicking materials will enable complex imaging phantoms for a wide range of microscopic and mesoscale optical imaging techniques.

Disclosures

The authors declare no conflicts of interest.

Acknowledgments

Funding sources include EPSRC Underpinning Multiuser Equipment EP/P030084/1, Innovative Engineering for Health award by the Wellcome Trust (WT101957) and the Engineering and Physical Sciences Research Council (EPSRC) (NS/A000027/1), Starting Grant from the European Research Council (ERC-2012-StG, Proposal 310970 MOPHIM), EPSRC First Grant (EP/J010952/1), by a Wellcome/EPSRC Centre award (203145Z/16/Z and NS/A000050/1), Royal Society Research Grant (RG160569), the UCL EPSRC Centre for Doctoral Training in Medical Imaging (EP/L016478/1), Starting Grant from the European Research Council (ERC-2012-StG, Proposal 679891 IntelGlazing), and UCL Overseas Research Scholarship and Dean's Award. This research was supported by the National Institute for Health Research University College London Hospitals Biomedical Research Centre. We thank the Centre for Nature Inspired Engineering for access to their facilities and Professor Marc-Olivier Coppens for useful conversations.

References

1. G. J. Tearney et al., "Consensus standards for acquisition, measurement, and reporting of intravascular optical coherence tomography studies," *J. Am. Coll. Cardiol.* **59**(12), 1058–1072 (2012).
2. H. Sinclair et al., "OCT for the identification of vulnerable plaque in acute coronary syndrome," *JACC Cardiovasc. Imaging* **8**(2), 198–209 (2015).
3. A. Fouad et al., "Variations in optical coherence tomography resolution and uniformity: a multi-system performance comparison," *Bio. Opt. Express* **5**(7), 2066–2081 (2014).
4. A. Curatolo et al., "Structured three-dimensional optical phantom for optical coherence tomography," *Opt. Express* **19**(12), 19480–19485 (2011).
5. G. Lamouche et al., "Review of tissue simulating phantoms with controllable optical, mechanical and structural properties for use in optical coherence tomography," *Bio. Opt. Express* **3**(6), 1381–1398 (2012).
6. C.-É. Bisaillon et al., "Artery phantoms for intravascular optical coherence tomography: healthy arteries," *Bio. Opt. Express* **2**(9), 2599–2613 (2011).
7. C.-É. Bisaillon and G. Lamouche, "Artery phantoms for intravascular optical coherence tomography: diseased arteries," *J. Biomed. Opt.* **18**(9), 096010 (2013).
8. B. F. Kennedy et al., "Fibrin phantom for use in optical coherence tomography," *J. Biomed. Opt.* **15**(3), 030507 (2010).
9. R. Bays et al., "Three-dimensional optical phantom and its application in photodynamic therapy," *Lasers Surg. Med.* **21**(3), 227–234 (1997).
10. A. Bykov et al., "Multilayer tissue phantoms with embedded capillary system for OCT and DOCT imaging," *Proc. SPIE* **8091**, 80911R (2011).
11. M. Wróbel et al., "Nanoparticle-free tissue-mimicking phantoms with intrinsic scattering," *Bio. Opt. Express* **7**(6), 2088–2094 (2016).
12. G. Lee et al., "Fabrication of healthy and disease-mimicking retinal phantoms with tapered foveal pits for optical coherence tomography," *J. Biomed. Opt.* **20**(8), 085004 (2015).
13. J. Baxi et al., "Retina-simulating phantom for optical coherence tomography," *J. Biomed. Opt.* **19**(2), 021106 (2014).
14. M. Wang et al., "3D printing method for freeform fabrication of optical phantoms simulating hetereogenous biological tissue," *Proc. SPIE* **8945**, 894509 (2014).
15. P. Diep et al., "Three-dimensional printed optical phantoms with customized absorption and scattering properties," *Bio. Opt. Express* **6**(11), 4212–4220 (2015).
16. K.-S. Lee et al., "Advances in 3D nano/microfabrication using two-photon initiated polymerization," *Prog. Polym. Sci.* **33**(6), 631–681 (2008).
17. P. van Assenbergh et al., "Nanostructure and microstructure fabrication: from desired properties to suitable processes," *Small* **14**(20), 1703401 (2018).
18. M. Power et al., "A monolithic force-sensitive 3D microgripper fabricated on the tip of an optical fiber using 2-photon polymerization," *Small* **14**(16), 1703964 (2018).
19. A. Accardo et al., "Multiphoton direct laser writing and 3D imaging of polymeric freestanding architectures for cell colonization," *Small* **13**(27), 1700621 (2017).
20. S. Wu et al., "Two-photon polymerisation for three-dimensional microfabrication," *J. Photochem. Photobiol. A: Chem.* **181**(1), 1–11 (2006).
21. M. Göppert-Mayer, "Über elementarakte mit zwei quantensprüngen," *Ann. Phys. (Leipzig)* **401**(3), 273–294 (1931).
22. D. B. Fullager et al., "Infrared dielectric response of nanoscribe IP-dip and IP-L monomers after polymerization from 250 cm^{-1} to 6000 cm^{-1}," *Opt. Mater. Express* **7**(3), 888–894 (2017).
23. T. Gissibl et al., "Sub-micrometre accurate free-form optics by three-dimensional printing on single-mode fibres," *Nat. Commun.* **7**, 11763 (2016).
24. J. Ramirez et al., "Low-loss modified SU-8 waveguides by direct laser writing at 405m," *Opt. Mater. Express* **7**(7), 2651–2659 (2017).
25. B. F. Kennedy et al., "Speckle reduction in optical coherence tomography images using tissue viscoelasticity," *J. Biomed. Opt.* **16**(2), 020506 (2011).
26. D. de Bruin et al., "Optical phantoms of varying geometry based on thin building blocks with controlled optical properties," *J. Biomed. Opt.* **15**(2), 025001 (2010).
27. G. Stone et al., "A prospective natural-history study of coronary atherosclerosis," *N. Engl. J. Med.* **364**, 226–235 (2011).
28. F. Gunstone, *Vegetable Oils in Food Technology Composition, Properties and Uses*, pp 170–177, Wiley, Hoboken, New Jersey (2011).
29. T. Gissibl et al., "Refractive index measurements of photo-resists for three-dimensional direct laser writing," *Opt. Mater. Express* **7**(7), 2293–2298 (2017).
30. S. Jacques, "Optical properties of biological tissues: a review," *Phys. Med. Biol.* **58**(11), R37 (2013).
31. A. Accardo et al., "Two-photon lithography and microscopy of 3D hydrogel scaffolds for neuronal cell growth," *Biomed. Phys. Eng. Express* **4**(2), 027009 (2018).
32. G. Calzetti et al., "Assessment of choroidal blood flow using laser speckle flowgraphy," *Br. J. Ophthalmol.* **102**(12), 1679–1683 (2018).
33. M. Degrand et al., "Tissue-like phantoms for near-infrared fluorescence imaging system assessment and the training of surgeons," *J. Biomed. Opt.* **11**(1), 014007 (2006).